Delft University of Technology

Document Version
Final published version

Licence
CC BY

Citation (APA)
Bosco, S., & Rimbach-Russ, M. (2026). Exchange-only spin-orbit qubits in silicon and germanium. *Physical Review Applied*, *25*(2), Article L021002. https://doi.org/10.1103/nl35-6886

Important note
To cite this publication, please use the final published version (if applicable).
Please check the document version above.

Copyright
In case the licence states “Dutch Copyright Act (Article 25fa)”, this publication was made available Green Open Access via the TU Delft Institutional Repository pursuant to Dutch Copyright Act (Article 25fa, the Taverne amendment). This provision does not affect copyright ownership.
Unless copyright is transferred by contract or statute, it remains with the copyright holder.

Sharing and reuse
Other than for strictly personal use, it is not permitted to download, forward or distribute the text or part of it, without the consent of the author(s) and/or copyright holder(s), unless the work is under an open content license such as Creative Commons.

Takedown policy
Please contact us and provide details if you believe this document breaches copyrights.
We will remove access to the work immediately and investigate your claim.

This work is downloaded from Delft University of Technology.

Letter

Exchange-only spin-orbit qubits in silicon and germanium

Stefano Bosco* and Maximilian Rimbach-Russ
QuTech and Kavli Institute of Nanoscience, Delft University of Technology, Delft, The Netherlands

(Received 7 October 2024; revised 24 December 2025; accepted 5 January 2026; published 10 February 2026)

The strong spin-orbit interaction in silicon and germanium hole quantum dots enables all-electric microwave control of single spins but is unsuited for multispin exchange-only qubits that rely on scalable discrete signals to suppress crosstalk and heating effects in large quantum processors. Here, we propose an exchange-only spin-orbit qubit that utilizes spin-orbit interactions to implement qubit gates and keeps the beneficial properties of the original encoding. Our encoding is robust to significant local variability in hole spin properties and, because it operates with two degenerate states, it eliminates the need for the rotating frame, avoiding the technologically demanding constraints of fast clocks and precise signal calibration. Unlike current exchange-only qubits, which require complex multistep sequences prone to leakage, our qubit design enables low-leakage two-qubit gates in a single step, addressing critical challenges in scaling spin qubits.

DOI: 10.1103/nl35-6886

Introduction. Hole spin qubits in silicon (Si) and germanium (Ge) quantum dots are leading candidates for large-scale quantum computers [1–14]. Their strong spin-orbit interaction (SOI) enables ultrafast all-electric operations [15–23] and strong coupling to microwave photons [24–30] without requiring bulky external micromagnets. The SOI also provides a means to control qubit properties *in situ*, offering sweet spots to enhance qubit performance [31–42].

Despite these advantages, most spin qubits, both electron- and hole-based, are still controlled by microwave driving [43–47]. This approach poses severe scalability challenges, including microwave crosstalk and heat dissipation, which limit the density and reliability of large quantum processors [48–51]. Alternative control using discrete electrical pulses would be more scalable, yet their realization for hole spins has remained limited, with only partial progress in systems based on spin hopping in Ge quantum dots [11,52]. These implementations still require fast clock calibration to track qubit precession in the rotating frame, introducing significant experimental complexity.

For electron-based qubits, an elegant way to overcome these issues is the exchange-only (XO) qubit [3,53–70]. By utilizing two degenerate $S = 1/2$ eigenstates of three exchange-coupled spins in three dots, quantum gates are implemented by tuning the exchange interaction between three spins using discrete voltage pulses, avoiding continuous driving and thereby suppressing crosstalk and heating. However, conventional XO qubits face two major limitations. First, their gate sequences are relatively complex and are prone to leakage into unwanted spin states that complicate error correction [3,53,59,70–79]. Second, the presence of low-lying valley states in Si disrupts the intended spin encoding [80–82].

Hole systems naturally circumvent the valley problem, but their strong SOI, while beneficial for electrical control, mixes different spin states and leads to anisotropic exchange interactions [12,13,83–87]. This anisotropy complicates the implementation of conventional XO-type encodings, which rely on isotropic exchange to achieve robust qubit operations.

In this work, we introduce an alternative XO encoding fully compatible with current technology that leverages the strong SOI of hole spins. Unlike current XO qubits, our exchange-only spin-orbit (XOSO) qubit, depicted in Fig. 1, is encoded in the crossing of energy eigenspaces with spin $S_z = -1/2$ and $S_z = -3/2$. In state-of-the-art devices, our encoding is robust against variability of local spin properties and removes the need for operating in the rotating frame, similar to XO qubits. In contrast to XO qubits, XOSO encoding allows full control via discrete signals because of SOI, and, importantly it also enables two-qubit entangling gates in a single step and is resilient to leakage. By mitigating critical issues of hole and XO qubits, our XOSO encoding represents a scalable path toward quantum computers.

XOSO qubit. We consider a system of three hole spins arranged in a linear array of quantum dots in Si or Ge, as illustrated in Figs. 1(a) and 1(b). The system is modeled by

*Contact author: s.bosco@tudelft.nl

Published by the American Physical Society under the terms of the Creative Commons Attribution 4.0 International license. Further distribution of this work must maintain attribution to the author(s) and the published article's title, journal citation, and DOI.

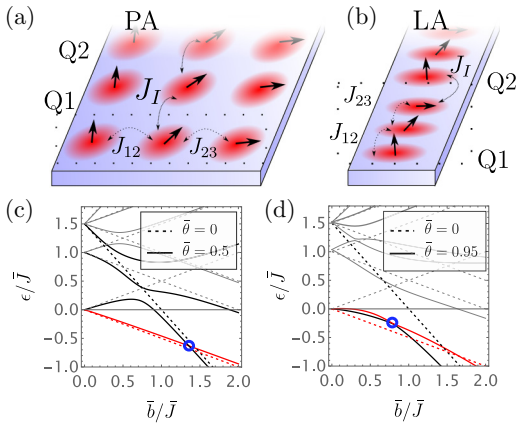

FIG. 1. Exchange-only spin-orbit (XOSO) qubits. (a),(b) Schematic of three quantum dots, each containing one hole spin, coupled by exchange interactions J_{ij}. These interactions are anisotropic due to the strong SOI, that tilts the spin quantization axes of different dots. XOSO qubits are arranged in planar (a) and linear (b) configurations. Two-qubit gates are achieved by activating the exchange coupling J_I. (c),(d) Energy spectrum ϵ against the average Zeeman energy $\bar{b}$ shown with (solid lines, $\bar{\theta} \neq 0$) and without SOI (dashed lines, $\bar{\theta} = 0$). The blue circle highlights the XOSO operating point. (c) Identical quantum dots with moderate SOI $\bar{\theta} = 0.5$ and no local variations of spin properties $\delta b_{ij} = \delta\theta_{ij} = \delta J = 0$. (d) Locally varying quantum dots with larger SOI $\bar{\theta} = 0.95$, angular variations $\delta\theta_{12} = 0.3$, and varying g-factors $g_1 = 0.1$, $g_2 = 0.15$, and $g_3 = 0.06$. For these experimentally relevant parameters in Si and Ge, the energy-level crossing occurs at $\delta J = 0.16\bar{J}$.

the qubit-frame Hamiltonian [12,13,83,84]

$$H = \sum_i \frac{b_i}{2}\sigma_z^{(i)} + \frac{J_{12}}{4}\boldsymbol{\sigma}^{(1)} \cdot \hat{R}_y(\theta_{12})\boldsymbol{\sigma}^{(2)} + \frac{J_{23}}{4}\boldsymbol{\sigma}^{(2)} \cdot \hat{R}_y(\theta_{23})\boldsymbol{\sigma}^{(3)}, \tag{1}$$

which comprises Zeeman energies $b_i = g_i\mu_B B$ and anisotropic exchange interactions J_{ij} between spins i and j. The effects of site-dependent g-tensors and spin-flip hopping induced by large SOI are captured by the three-dimensional rotation matrix $\hat{R}_y(\theta_{ij})$. We introduce the average and difference of Zeeman energies $\bar{b} = \sum_i b_i/3$ and $\delta b_{ij} = (b_i - b_j)/2$, respectively. Similarly, for the exchange interactions, we define $\bar{J} = (J_{12} + J_{23})/2$, $\delta J = (J_{12} - J_{23})/2$, and $\bar{\theta} = (\theta_{12} + \theta_{23})/2$, $\delta\theta = (\theta_{12} - \theta_{23})/2$. Equation (1) accurately describes three spins in Si and Ge triple dots [12,83], where effects of higher-energy states [88,89] and additional cubic anisotropies [86,87] are small. For more details and a microscopic derivation of H, see the Supplemental Material [90].

The energy spectrum for two distinct cases is shown in Figs. 1(c) and 1(d). Without magnetic field ($b_i = 0$), the three interacting spins form two doublets with spin $S = 1/2$ separated by $\bar{J}$ and a quartet with spin $S = 3/2$ positioned at $3\bar{J}/2$ above the lowest doublet [53,54,59]. As $\bar{b}$ increases, the spin $S_z = -3/2$ state rapidly lowers its energy, eventually becoming the ground state. Importantly, the $S_z = -3/2$ and the low-energy $S_z = -1/2$ states *cross* [see the blue circles in Figs. 1(c) and 1(d)]. This energy crossing is present even for large SOI and local variability, giving rise to a degenerate subspace that defines the operating point of our XOSO qubit.

For identical quantum dots and moderate SOI $\bar{\theta}$s, the crossing occurs at $\bar{b}/\bar{J} = 3/2 - 23\bar{\theta}^2/40 + \mathcal{O}(\bar{\theta}^4)$ [see Fig. 1(c)]. Although larger values of $\bar{\theta}$ hybridize different spin sectors and significantly impact the energy spectrum, for $\bar{\theta} \leq \pi/2$, the crossing between the ground and first states persists, albeit shifted to lower $\bar{b}/\bar{J}$ ratios.

Remarkably, this crossing is robust against local variations of system parameters. While finite values of δb_{ij} and $\delta\theta$ split the degeneracy of our qubit if $J_{12} = J_{23}$, the energy crossing is restored when $J_{12} \neq J_{23}$ by locally adjusting the exchange between different dots. As shown in Fig. 1(d), the relative exchange δJ exactly compensates for large δb_{ij} and $\delta\theta$, extending the validity of our encoding also to extreme regimes with comparable values of average and relative dot parameters. However, our qubit is susceptible to local misalignment of rotation axes of the two exchanges ($J_{23}R_y \to J_{23}R_{y+\delta\phi}$), which creates a small gap proportional to $\delta\phi$ at the XOSO operating point and arises from relative tilts of SOI and out-of-plane g-tensors in nanowires and planar Ge, respectively. Because in most experiments, $\bar{b} \gg \delta b_{ij}$, $\bar{\theta} \gg \delta\theta$ [12,13,20–22,32,83], and $\delta\phi \sim 1^\circ$ [32], below we neglect local variations and small gaps, which can be efficiently compensated by dynamical decoupling. See the Supplemental Material for more details on the stability of XOSO qubits [90].

Qubit states. We encode our XOSO qubit in the twofold degenerate subspace where the ground and first excited states cross [blue circles in Figs. 1(c) and 1(d)]. Unlike current hole spin qubits and similar to XO qubits, the degeneracy of the energy states ensures that our qubit has no constant dynamics, significantly simplifying control by eliminating the need for fast clocks to synchronize qubit operations [53,66,91,92]. For small $\bar{\theta}$s, our computational subspace is approximately spanned by the qubit states

$$|0\rangle \approx |\downarrow\downarrow\downarrow\rangle, \tag{2a}$$

$$|1\rangle \approx \frac{|\uparrow\downarrow\downarrow\rangle + |\downarrow\downarrow\uparrow\rangle}{\sqrt{6}} - \sqrt{\frac{2}{3}}|\downarrow\uparrow\downarrow\rangle. \tag{2b}$$

This decomposition shows that our XOSO qubit can be initialized and readout via Pauli spin blockade (PSB) [9,11,93–102]. In holes, PSB differentiates $|\downarrow\downarrow\rangle$ pairs from remaining states [103], thus similar to variants of

XO qubits [104], the XOSO states are completely distinguished by two PSB measurements executed sequentially on the $(1,2)$ and $(2,3)$ dot pairs.

For isotopically purified materials and in-plane magnetic field hyperfine noise is suppressed [32,41,105], and we expect decoherence to arise from random fluctuations of the exchange energy caused by charge noise. Although these couple directly to the qubit, similar to XO qubits [59], they can be mitigated by operating at the symmetric point with zero detunings. Here, the system is protected against the dominant fluctuations of detunings [3]. Fluctuations of gate potentials V with standard deviation σ_V still couple to J, resulting in the dephasing rate $1/T_2^* \sim \sigma_V \partial_V J/h$. Current experiments operate at small exchanges approximated by $J = J_0 e^{\kappa V} \sim 50\,\mathrm{MHz}$. At $V = 80\,\mathrm{mV}$, $\sigma_V = 0.8\,\mathrm{mV}$, $\kappa = 0.06/\mathrm{mV}$, and $J_0/h = 0.24\,\mathrm{MHz}$ [11], we estimate $T_2^* \sim 0.7\,\mu\mathrm{s}$, comparable with electron-based XO qubits [66]. Similar to Si and GaAs heterostructures [66,106], at larger J-values, approaching the gigahertz range, we expect the sensitivity $\partial_V \bar{J}$ to vanish, dramatically improving coherence. We also envision improvement by dynamical decoupling schemes [70,107–109]. Also, at the symmetric point we have $J \propto t^2$ [90], enabling single- and two-qubit gates by modulating the tunneling t between dots [11,110].

Single-qubit gates. At the degeneracy point, the SOI $\bar{\theta}$ enables the two orthogonal axes of control necessary for single-qubit operations via global and relative exchange coupling. The XOSO qubit Hamiltonian, to lowest order in $\bar{\theta}$, is given by

$$H_{\mathrm{XOSO}} = -\frac{3\bar{j}(t)}{4}\tau_z - \bar{\theta}\sqrt{\frac{3}{2}}\frac{3\delta j(t)}{4}\tau_x, \tag{3}$$

where the Pauli matrices τ_i act on the qubit subspace, and $\bar{j}(t) = [J_{12}(t) + J_{23}(t)]/2 - \bar{J}$ and $\delta j(t) = [J_{12}(t) - J_{23}(t)]/2 - \delta J$ are the deviation of global and relative exchange coupling from the static values $\bar{J}$ and δJ that define our degenerate qubit [blue circles in Figs. 1(c) and 1(d)]. Higher-order corrections in $\bar{\theta}$, δb_{ij}, and $\delta\theta$, alter the driving terms only quantitatively (see the Supplemental Material [90]).

We consider Si and Ge hole spin qubits, where $\bar{\theta}$ can be engineered to approach even π [12]. However, because our analysis is constrained to small values of $\bar{\theta}$, we limit the discussion to moderate values $\bar{\theta} \sim 0.5 \sim 30^\circ$. These values still enables fast electric driving, and are routinely achieved experimentally in Ge double dots with in-plane magnetic field [32,83].

In Fig. 2(a), we show the time evolution of the operators τ_x (blue) and τ_z (red), obtained by suddenly turning on $\delta j/h$ and $\bar{j}/h$ with a baseband pulse with amplitude 20 MHz. The simulation of the full 2^3-dimensional Hamiltonian H in Eq. (1) aligns well with the behavior predicted by the effective XOSO Hamiltonian in H_{XOSO} Eq. (3), enabling single-qubit operations in tens of nanoseconds.

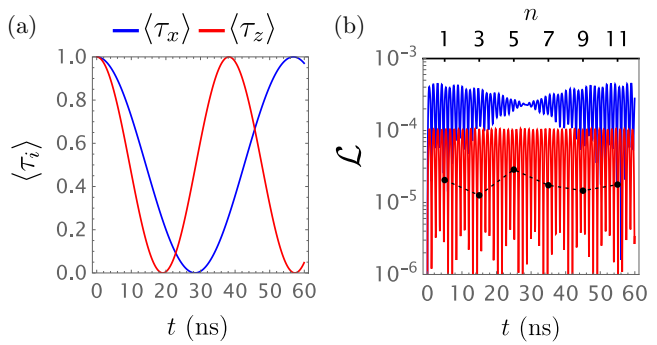

FIG. 2. Single-qubit gates. (a) The expectation value of τ_x (τ_z) generated by a rectangular pulse with amplitude 20 MHz that activates $\delta j/h$ ($\bar{j}/h$) for a time t is shown in blue (red) lines. The initial states are $|0\rangle$ ($|+\rangle = (|0\rangle + |1\rangle)/\sqrt{2}$). We use $\bar{\theta} = 0.5 \approx 30^\circ$ and $\bar{J}/h \approx 1\,\mathrm{GHz}$. (b) Leakage $\mathcal{L}$ from the computational space. Blue and red lines correspond to the leakage over time t generated by the respective single-qubit gates in (a). The black dots represent the leakage during the $_\varphi$SWAP two-qubit gate, plotted against the dimensionless index $n \propto t$, corresponding to the black dots in Fig. 3(b).

Leakage. Unlike XO qubits, where leakage is a critical challenge [3,59], the always-on exchange interaction $\bar{J}$ in XOSO qubits separates the computational and noncomputational subspaces, effectively suppressing leakage. We quantify leakage during single-qubit gates by simulating the time evolution of Eq. (1) and calculating the probability of ending in non-computational states for initial states chosen from the six cardinal points of the Bloch sphere. Specifically, the leakage is $\mathcal{L} = 1 - \sum_i^N \sum_{j=0,1} |\langle j|e^{-iHt/\hbar}|i\rangle)|^2/N$, where $N = 6$.

In Fig. 2(b), we demonstrate that, under realistic parameters, leakage is substantially reduced in our system. For an X (Z) gate, the leakage scales roughly as $\delta j^2/\bar{J}^2$ ($\bar{j}^2/\bar{J}^2$), meaning that exchange-pulse amplitude and gate time are determined by $\bar{J}$. Crucially, leakage is also suppressed during two-qubit gates. We straightforwardly extended our simulation (black points) to model six interacting spins (see Fig. 1), incorporating Bell states as initial states. Because noncomputational states remain gapped by approximately $\bar{J}$ even when inter-qubit exchange interaction J_I is activated, low-leakage two-qubit gates are achieved for $J_I \ll \bar{J}$.

Finally, we note that our simulations use simple square pulses to toggle the interactions. By employing smoother pulses [111], leakage can be further reduced.

Two-qubit gates. A critical advantage of our XOSO qubit is the ability to implement different high-fidelity, low-leakage two-qubit gates using a single exchange pulse, which contrasts sharply with XO qubits [53,59,62,71,72].

We consider two distinct coupling schemes, the planar arrangement (PA) and linear arrangement (LA) of dots [see Figs. 1(a) and 1(b)]. In the PA, the exchange interaction $J_I(t)$ is activated between the central dots, while in the LA, interactions are restricted to the side dots.

For both configurations, we find a qubit-qubit interaction Hamiltonian H_I from the six-spin system by tracing out the high-energy noncomputational states by a Schrieffer-Wolff transformation. To lowest order in SOI,

$$H_I = \frac{J_I(t)}{8}\left[\alpha_H \boldsymbol{\tau}^{(1)}\cdot\boldsymbol{\tau}^{(2)} - \alpha_z\left(\tau_z^{(1)}\tau_z^{(2)} - \tau_z^{(1)} - \tau_z^{(2)}\right)\right]. \tag{4}$$

H_I contains Heisenberg-like ($\propto \boldsymbol{\tau}^{(1)}\cdot\boldsymbol{\tau}^{(2)}$) and Ising-like ($\propto \tau_z^{(1)}\tau_z^{(2)}$) exchange terms, as well as single-qubit terms ($\propto \tau_z^{(i)}$), where $\tau^{(i)}$ acts on qubit i. The dimensionless prefactors for PA are $\alpha_H^P = 4/3$, $\alpha_z^P = 4/9$, while for LA $\alpha_H^L = 1/3$, $\alpha_z^L = 5/18$.

Applying $J_I(t)$ for a time t using a square pulse with amplitude $J_I = h/\tau_I$ leads to the time evolution

$$U_I = \begin{pmatrix} 1 & 0 & 0 & 0 \\ 0 & \frac{1}{2}\left(1+e^{\frac{i\pi t\alpha_H}{\tau_I}}\right) & \frac{1}{2}\left(1-e^{\frac{i\pi t\alpha_H}{\tau_I}}\right) & 0 \\ 0 & \frac{1}{2}\left(1-e^{\frac{i\pi t\alpha_H}{\tau_I}}\right) & \frac{1}{2}\left(1+e^{\frac{i\pi t\alpha_H}{\tau_I}}\right) & 0 \\ 0 & 0 & 0 & e^{\frac{i\pi t\alpha_z}{\tau_I}} \end{pmatrix}. \tag{5}$$

When $t = T_{\text{gate}} = n\tau_I/\alpha_H$, with integer n, U_I produces a family of entangling gates. For even n, U_I is diagonal and generates a controlled-phase gate $\text{cP}_\phi = \text{diag}(1,1,1,e^{i\phi})$ with $\phi = \pi n\alpha_z/\alpha_H$. For odd n, the cP is combined with a SWAP gate, $U_I = \text{SWAP}\cdot\text{cP}_\phi$.

The gate time T_{gate} and the phase ϕ depend on the coupling scheme. For PA $\phi^P = \pi n/3$, and for LA $\phi^L = 5\pi n/6$. The gate time is $T_{\text{gate}}^P = 4T_{\text{gate}}^L = 3n\tau_I/4$. Remarkably, for LA, when $n = 6$ our XOSO qubits implement a controlled-Z gate with a single pulse, without requiring additional single-qubit rotations. However, the PA enables gates that are four times faster. For example, using an exchange pulse with moderate amplitude $J_I/h = 20\,\text{MHz}$, which ensures low leakage [see Fig.2(b)], fast two-qubit gates are achieved in $T_{\text{gate}}^P/n \approx 37.5\,\text{ns}$ and $T_{\text{gate}}^L/n \approx 150\,\text{ns}$. Interestingly, in addition to faster gates, the PA also enables higher-fidelity operations.

Gate fidelity. While we require SOI within dots comprising the qubit, SOI between dots belonging to different qubits can induce systematic two-qubit gate errors. Importantly, careful dot engineering can reduce interqubit SOI θ_I while maintaining intraqubit SOI $\bar{\theta}$ [37,112–120].

Interqubit SOI θ_I causes the small correction to the two-qubit interaction Hamiltonian

$$H_I^1 = \frac{J_I(t)\theta_I}{3\sqrt{6}}\left[\alpha_x\left(\tau_x^{(1)} - \tau_x^{(2)}\right) - \alpha_{\text{dm}}\left(\boldsymbol{\tau}^{(1)}\times\boldsymbol{\tau}^{(2)}\right)\cdot\boldsymbol{e}_y\right], \tag{6}$$

comprising Dzyaloshinskii-Moriya interactions (proportional to α_{dm}) and single-qubit terms (proportional to α_x). For PA $\alpha_{\text{dm}}^P = 1$, $\alpha_x^P = 1/2$, and for LA $\alpha_{\text{dm}}^L = 7\bar{\theta}/20\theta_I - 1/8$, $\alpha_x^L = 2\bar{\theta}/5\theta_I - 5/8$.

The term α_{dm} introduces additional entanglement between qubits that is not captured by the original gate evolution U_I. Although these interactions may help engineering other gates, our focus is on enhancing the fidelity of the gate U_I. In PA, for isotropic interqubit interaction with $\theta_I^P = 0$, the correction H_I^1 vanishes. This condition can be reached, for example, by engineering dot shape and strain fields or by appropriately aligning the qubits with the SOI vector. Notably, these results hold even when the XOSO qubits have different values of $\bar{\theta}$. In LA, we can eliminate α_{dm}^L by setting $\theta_I^L = 14\bar{\theta}/5$, which can be done by tuning the dot positions. Any residual single-qubit dynamics can be compensated with synchronized pulses, such that $\delta j^{(1)} = -\delta j^{(2)} = J_I/5$.

There are second-order SOI corrections that renormalize Eq. (4) such that $\alpha_{H,z} \to \alpha_{H,z} - \bar{\theta}^2\alpha_{H,z}^{(2)}$. These corrections also generate the terms

$$H_I^2 = \frac{J_I(t)\bar{\theta}^2}{4}\left[\alpha_y\tau_y^{(1)}\tau_y^{(2)} + \frac{\delta\alpha_z}{2}\left(\tau_z^{(1)} + \tau_z^{(2)}\right)\right]. \tag{7}$$

For PA at $\theta_I^P = 0$, we find $[\alpha_H^{(2)}]^P = 437/450$, $[\alpha_z^{(2)}]^P = 227/270$, $\alpha_y^P = 1/3$, $\delta\alpha_z^P = 22/675$, and at $\theta_I^L = 14\bar{\theta}/5$ for LA, $[\alpha_H^{(2)}]^L = 1259/1800$, $[\alpha_z^{(2)}]^L = 4837/5400$, $\alpha_y^L = 287/600$, $\delta\alpha_z^L = 1789/2700$.

The full time-evolution operator U including H_I^2 factorizes as $U = U_I U_2$, where U_I is given in Eq. (5). The additional dynamics U_2 includes SWAP transitions between $|01\rangle$ and $|10\rangle$ states with frequency $\bar{\theta}^2\alpha_y/4\tau_I$ and double spin-flip transitions between $|00\rangle$ and $|11\rangle$ with frequency $\Omega/4\tau_I$, with $\Omega = \sqrt{\beta_z^2 + \alpha_y^2\theta^4}$, and amplitude $\bar{\theta}^2\alpha_y/\Omega$. To simplify the notation, we reabsorb the corrections $\alpha_{H,z}^{(2)}$ into $\alpha_{H,z}$, and we introduce the prefactor $\beta_z = \alpha_z + \bar{\theta}^2\delta\alpha_z$ of the single-particle term proportional to $\tau_z^{(1)} + \tau_z^{(2)}$. The full form of U is given in the Supplemental Material [90].

The two-qubit gate fidelity is extracted from the explicit form of U at $t = n\tau_I/\alpha_H$ as

$$\mathcal{F} = \left|\frac{1}{4}\text{Tr}(U_I^\dagger U)\right|^2 \approx 1 - C_n\bar{\theta}^4, \tag{8}$$

where the constant $C_n \sim n^2$ depends on the coupling scheme [90]. Figure 3(a) shows a comparison of $\mathcal{F}$ for LA

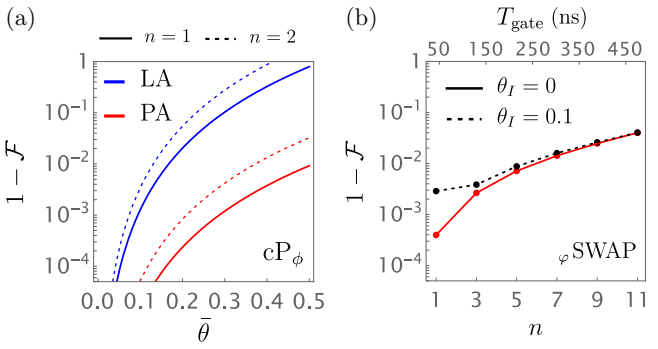

FIG. 3. Two-qubit gates. (a) Infidelity $1-\mathcal{F}$ of the cP_ϕ gate for the planar arrangement (PA) and linear arrangement (LA) of dots [see Figs. 1(a) and 1(b)] against $\bar{\theta}$. We consider a pulse duration of $t=n\tau_I/\alpha_H$ with $n=1$ (solid lines) and $n=2$ (dashed lines). Specifically, for PA (LA) with pulse amplitude $J_I/h=20\,\mathrm{MHz}$, the gate time is $T_{\mathrm{gate}}=\tau_I/\alpha_H\approx 37\,\mathrm{ns}$ ($T_{\mathrm{gate}}\approx 150\,\mathrm{ns}$). (b) Infidelity of the ${}_\varphi\mathrm{SWAP}$ gate against n for $\theta_I=0$ (red) and $\theta_I=0.1\approx 6^\circ$ (black). We simulate the full time evolution of the six spins in PA using $\bar{J}/h=1\,\mathrm{GHz}$, $\bar{\theta}=0.5$, and $J_I/h=20\,\mathrm{MHz}$.

and PA across different n values. PA provides faster gates and higher fidelity.

SOI-enabled two-qubit gates. Interestingly, H_I^2 (7) also enables two-qubit gates resilient to third-order SOI effects. By applying a pulse with $\bar{j}^{(1)}=\bar{j}^{(2)}=\bar{j}$, we can tune single-qubit terms to $\beta_z\to\beta_z^*=\beta_z+6\bar{j}/J_I$, and the double-spin-flip frequency $\Omega\to\Omega^*=\sqrt{(\beta_z^*)^2+\bar{\theta}^4\alpha_y^2}$. This permits synchronizing SWAP and double-spin-flip oscillations. Choosing $\bar{j}$ such that $\Omega^* t=2\tau_I$, at $t=T_{\mathrm{gate}}=n\tau_I/(\alpha_H+\bar{\theta}^2\alpha_y)$, with odd n, results in the phase SWAP

$$ {}_\varphi\mathrm{SWAP}=\begin{pmatrix}1&0&0&0\\0&0&e^{i\varphi}&0\\0&e^{i\varphi}&0&0\\0&0&0&1\end{pmatrix}, \tag{9}$$

with phase $\varphi/\pi=1-n(\alpha_z+\alpha_y\bar{\theta}^2)/2(\alpha_H+\alpha_y\bar{\theta}^2)$. For PA and LA, we find $\varphi^P/\pi-1\approx -n(1/6-199\bar{\theta}^2/1800)$ and $\varphi^L/\pi-1\approx -n(5/12-1259\bar{\theta}^2/3600)$, respectively.

We confirm numerically that this class of two-qubit gates achieves high fidelity by simulating the dynamics of six interacting spins under the appropriate $\bar{j}$ pulse. Figure 3(b) focuses on the PA with a pulse $J_I/h=20\,\mathrm{MHz}$ and $\bar{\theta}=0.5$, illustrating the infidelity arising from higher-order SOI corrections and finite θ_I. This entangling gate can be implemented at high speed, high fidelity, and low leakage [see Fig. 2(b)].

We anticipate that gate fidelities can be enhanced with various techniques, as SOI is highly tunable via dot and strain engineering [34,37,112–120], enabling protocols switching off SOI during two-qubit gates to eliminate systematic errors, while pulse shaping and dynamical decoupling can further improve performance [111,121,122].

Conclusion. We introduce the XOSO qubit, comprising three spins located in hole quantum dots. Our encoding is fully compatible with current technology, leverages strong SOI to enable qubit control using discrete signals, removes the need for fast clocks, and significantly reduces critical challenges for scaling up quantum devices. In contrast to XO qubits, our XOSO qubits are intrinsically protected against leakage during qubit operations, allowing fast high-fidelity two-qubit entangling gates with a single pulse. This makes XOSO qubits a promising scalable alternative for large-scale quantum processors.

Acknowledgement. We thank Tess Vakhtel, Barnaby Van Straaten, and Damien Crielaard for insightful discussions. This research was partly supported by the EU through the H2024 QLSI2 project and partly sponsored by the Army Research Office under Award No. W911NF-23-1-0110. M.R.-R. acknowledges additional support from NWO under Veni Grant VI.Veni.212.223. The views and conclusions contained in this article are those of the authors and should not be interpreted as representing the official policies, either expressed or implied, of the Army Research Office or the US Government. The US Government is authorized to reproduce and distribute reprints for Government purposes notwithstanding any copyright notation herein.

Data Availability. The data that support the findings of this article are not publicly available. The data are available from the authors upon reasonable request.

[1] D. Loss, *et al.*, Phys. Rev. A **57**, 120 (1998).
[2] G. Burkard, *et al.*, Phys. Rev. B **59**, 2070 (1999).
[3] G. Burkard, *et al.*, Rev. Mod. Phys. **95**, 025003 (2023).
[4] P. Stano, *et al.*, Nat. Rev. Phys. **4**, 672 (2022).
[5] G. Scappucci, *et al.*, Nat. Rev. Mater. **6**, 926 (2021).
[6] C. Kloeffel, *et al.*, Annu. Rev. Condens. Matter Phys. **4**, 51 (2013).
[7] Y. Fang, *et al.*, Mater. Quantum Technol. **3**, 012003 (2023).
[8] R. Maurand, *et al.*, Nat. Commun. **7**, 13575 (2016).
[9] N. W. Hendrickx, *et al.*, Nature **591**, 580 (2021).
[10] F. Borsoi, *et al.*, Nat. Nanotechnol. **19**, 21 (2024).
[11] C.-A. Wang, *et al.*, Science **385**, 447 (2024).
[12] S. Geyer, *et al.*, Nat. Phys. **20**, 1152 (2024).
[13] X. Zhang, *et al.*, Nat. Nanotechnol. **20**, 209 (2025).
[14] V. John, *et al.*, Nat. Commun. **16**, 10560 (2025).
[15] D. V. Bulaev, *et al.*, Phys. Rev. Lett. **98**, 097202 (2007).
[16] N. W. Hendrickx, *et al.*, Nat. Commun. **11**, 3478 (2020).
[17] F. N. M. Froning, *et al.*, Nat. Nanotechnol. **16**, 308 (2021).
[18] K. Wang, *et al.*, Nat. Commun. **13**, 206 (2022).
[19] L. C. Camenzind,*et al.*, Nat. Electron. **5**, 178 (2022).

[20] D. Jirovec, *et al.*, Nat. Mater. **20**, 1106 (2021).
[21] D. Jirovec, *et al.*, Phys. Rev. Lett. **128**, 126803 (2022).
[22] S. D. Liles, *et al.*, Nat. Commun. **15**, 7690 (2024).
[23] H. Liu, *et al.*, Nano Lett. **23**, 3810 (2023).
[24] C. X. Yu, *et al.*, Nat. Nanotechnol. **18**, 741 (2023).
[25] F. De Palma, *et al.*, Nat. Commun. **15**, 10177 (2024).
[26] S. Bosco, *et al.*, Phys. Rev. Lett. **129**, 066801 (2022).
[27] C. Kloeffel, *et al.*, Phys. Rev. B **88**, 241405(R) (2013).
[28] V. P. Michal, *et al.*, Phys. Rev. B **107**, L041303 (2023).
[29] P. M. Mutter, *et al.*, Phys. Rev. Res. **3**, 013194 (2021).
[30] M. Rimbach-Russ, *et al.*, Phys. Rev. Lett. **135**, 197001 (2025).
[31] N. Piot, *et al.*, Nat. Nanotechnol. **17**, 1072 (2022).
[32] N. W. Hendrickx, *et al.*, Nat. Mater. **23**, 920 (2024).
[33] M. J. Carballido, *et al.*, Nat. Commun. **16**, 7616 (2025).
[34] S. Bosco, *et al.*, PRX Quantum **2**, 010348 (2021).
[35] Z. Wang, *et al.*, npj Quantum Inf. **7**, 54 (2021).
[36] S. Bosco, *et al.*, Phys. Rev. Appl. **18**, 044038 (2022).
[37] C.-A. Wang, *et al.*, npj Quantum Inf. **10**, 102 (2024).
[38] A. Sen, *et al.*, Phys. Rev. B **108**, 245406 (2023).
[39] L. Mauro, *et al.*, Phys. Rev. B **109**, 155406 (2024).
[40] S. Bosco, *et al.*, PRX Quantum **5**, 020353 (2024).
[41] S. Bosco, *et al.*, Phys. Rev. Lett. **127**, 190501 (2021).
[42] P. M. Mutter, *et al.*, Phys. Rev. B **104**, 195421 (2021).
[43] H. Watzinger, *et al.*, Nat. Commun. **9**, 3902 (2018).
[44] N. W. Hendrickx, *et al.*, Nature **577**, 487 (2020).
[45] S. Bosco, *et al.*, Phys. Rev. Lett. **131**, 197001 (2023).
[46] V. John, *et al.*, Phys. Rev. Lett. **132**, 067001 (2024).
[47] A. Crippa, *et al.*, Phys. Rev. Lett. **120**, 137702 (2018).
[48] B. Undseth, *et al.*, Phys. Rev. X **13**, 041015 (2023).
[49] J. Krupka, *et al.*, Appl. Phys. Lett. **107**, 082105 (2015).
[50] L. M. K. Vandersypen, *et al.*, npj Quantum Inf. **3**, 34 (2017).
[51] J. M. Boter, *et al.*, Phys. Rev. Appl. **18**, 024053 (2022).
[52] F. van Riggelen-Doelman, *et al.*, Nat. Commun. **15**, 5716 (2024).
[53] D. P. DiVincenzo, *et al.*, Nature **408**, 339 (2000).
[54] E. A. Laird, *et al.*, Phys. Rev. B **82**, 075403 (2010).
[55] L. Gaudreau, *et al.*, Nat. Phys. **8**, 54 (2012).
[56] A. Pal, *et al.*, Phys. Rev. X **4**, 011012 (2014).
[57] J.-T. Hung, *et al.*, Phys. Rev. B **90**, 045308 (2014).
[58] K. Eng, *et al.*, Sci. Adv. **1**, e1500214 (2015).
[59] M. Russ, *et al.*, J. Phys.: Condens. Matter **29**, 393001 (2017).
[60] J. Medford, *et al.*, Phys. Rev. Lett. **111**, 050501 (2013).
[61] J. M. Taylor, *et al.*, Phys. Rev. Lett. **111**, 050502 (2013).
[62] A. C. Doherty, *et al.*, Phys. Rev. Lett. **111**, 050503 (2013).
[63] J. Medford, *et al.*, Nat. Nanotechnol. **8**, 654 (2013).
[64] Y.-P. Shim, *et al.*, Phys. Rev. B **93**, 121410(R) (2016).
[65] A. J. Landig, *et al.*, Nature **560**, 179 (2018).
[66] A. J. Weinstein *et al.*, Nature **615**, 817 (2023).
[67] J. Z. Blumoff *et al.*, PRX Quantum **3**, 010352 (2022).
[68] E. Acuna, *et al.*, Phys. Rev. Appl. **22**, 044057 (2024).
[69] S. Mehl, *et al.*, Phys. Rev. B **87**, 195309 (2013).
[70] B. Sun *et al.*, PRX Quantum **5**, 020356 (2024).
[71] D. Zeuch, *et al.*, Phys. Rev. B **90**, 045306 (2014).
[72] F. Setiawan, *et al.*, Phys. Rev. B **89**, 085314 (2014).
[73] G. T. Hickman, *et al.*, Phys. Rev. B **88**, 161303(R) (2013).
[74] A. Sala, *et al.*, Phys. Rev. B **95**, 241303(R) (2017).
[75] M. Russ, *et al.*, Phys. Rev. Lett. **121**, 177701 (2018).
[76] C. Jones, *et al.*, Phys. Rev. X **8**, 021058 (2018).
[77] R. W. Andrews, *et al.*, Nat. Nanotechnol. **14**, 747 (2019).
[78] A. Pan, *et al.*, Quantum Sci. Technol. **5**, 034005 (2020).
[79] J. Kerckhoff, *et al.*, PRX Quantum **2**, 010347 (2021).
[80] F. A. Zwanenburg, *et al.*, Rev. Mod. Phys. **85**, 961 (2013).
[81] B. Koiller, *et al.*, Phys. Rev. Lett. **88**, 027903 (2001).
[82] D. Buterakos, *et al.*, PRX Quantum **2**, 040358 (2021).
[83] J. Saez-Mollejo, *et al.*, Nat. Commun. **16**, 3862 (2025).
[84] M. Spethmann, *et al.*, Phys. Rev. B **109**, 085303 (2024).
[85] B. Hetényi, *et al.*, Phys. Rev. Res. **2**, 033036 (2020).
[86] G. Katsaros, *et al.*, Nano Lett. **20**, 5201 (2020).
[87] B. Hetényi, *et al.*, Phys. Rev. Lett. **129**, 116805 (2022).
[88] M. T. P. Nguyen, *et al.*, PRX Quantum **6**, 030326 (2025).
[89] M. J. Rodríguez, *et al.*, Phys. Rev. B **112**, 115428 (2025).
[90] See Supplemental Material at http://link.aps.org/supplemental/10.1103/nl35-6886, where we report complete expressions for the effective qubit Hamiltonian including locally varying quantum-dot parameters, and the complete form of the two-qubit time-evolution operator and fidelity discussed in the main text.
[91] Y.-P. Shim, *et al.*, Nat. Commun. **7**, 11059 (2016).
[92] D. K. Weiss, *et al.*, PRX Quantum **3**, 040336 (2022).
[93] K. Takeda, *et al.*, npj Quantum Inf. **10**, 22 (2024).
[94] G. A. Oakes *et al.*, Phys. Rev. X **13**, 011023 (2023).
[95] D. J. Niegemann, *et al.*, PRX Quantum **3**, 040335 (2022).
[96] J. Danon, *et al.*, Phys. Rev. B **80**, 041301(R) (2009).
[97] M. Brauns, *et al.*, Phys. Rev. B **94**, 041411(R) (2016).
[98] A. E. Seedhouse, *et al.*, PRX Quantum **2**, 010303 (2021).
[99] F. Fehse, *et al.*, Phys. Rev. B **107**, 245303 (2023).
[100] D. Fernández-Fernández, *et al.*, Phys. Rev. Appl. **18**, 054090 (2022).
[101] N. S. Lai, *et al.*, Sci. Rep. **1**, 110 (2011).
[102] C. Ventura-Meinersen, *et al.*, EPJ Quantum Technol. **12**, 125 (2025).
[103] E. G. Kelly, *et al.*, arXiv:2504.06898.
[104] N. L. Foulk, *et al.*, Phys. Rev. Lett. **135**, 106202 (2025).
[105] J. Fischer, *et al.*, Phys. Rev. B **78**, 155329 (2008).
[106] O. E. Dial, *et al.*, Phys. Rev. Lett. **110**, 146804 (2013).
[107] L. Cywiński, *et al.*, Phys. Rev. B **77**, 174509 (2008).
[108] N. Rohling, *et al.*, Phys. Rev. B **93**, 205434 (2016).
[109] J. R. West, *et al.*, New J. Phys. **14**, 083002 (2012).
[110] A. S. Ivlev, *et al.*, Phys. Rev. X **15**, 031042 (2025).
[111] M. Rimbach-Russ, *et al.*, Quantum Sci. Technol. **8**, 045025 (2023).
[112] S. Bosco, *et al.*, Phys. Rev. B **104**, 115425 (2021).
[113] C. Kloeffel, *et al.*, Phys. Rev. B **97**, 235422 (2018).
[114] C. Adelsberger, *et al.*, Phys. Rev. B **105**, 075308 (2022).
[115] C. Adelsberger, *et al.*, Phys. Rev. B **106**, 235408 (2022).
[116] S. D. Liles, *et al.*, Phys. Rev. B **104**, 235303 (2021).
[117] J. C. Abadillo-Uriel, *et al.*, Phys. Rev. Lett. **131**, 097002 (2023).
[118] L. A. Terrazos, *et al.*, Phys. Rev. B **103**, 125201 (2021).
[119] A. Sarkar, *et al.*, Phys. Rev. B **108**, 245301 (2023).
[120] E. Valvo, *et al.*, arXiv:2512.12702.
[121] L. S. Theis, *et al.*, Europhys. Lett. **123**, 60001 (2018).
[122] İ. Polat, *et al.*, arXiv:2508.02902.